

# Actin Polymerization Kinetics, Cap Structure and Fluctuations

Ben O'Shaughnessy<sup>†</sup>\*, Dimitrios Vavylonis<sup>†</sup>, and Qingbo Yang<sup>‡</sup>

Departments of <sup>†</sup>Chemical Engineering and <sup>‡</sup>Physics, Columbia University, New York, NY 10027, USA

**Polymerization of actin proteins into dynamic structures is essential to eukaryotic cell life. This has motivated a large body of in vitro experiments measuring polymerization kinetics of individual filaments. Here we model these kinetics, accounting for all relevant steps revealed by experiment: polymerization, depolymerization, random ATP hydrolysis and release of phosphate (Pi). We relate filament growth rates to the dynamics of ATP-actin and ADP-Pi-actin caps which develop at filament ends. At the critical concentration of the barbed end,  $c_{\text{crit}}$ , we find a short ATP cap and a long fluctuation-stabilized ADP-Pi cap. We show that growth rates and the critical concentration at the barbed end are intimately related to cap structure and dynamics. Fluctuations in filament lengths are described by the length diffusion coefficient,  $D$ . Recently Fujiwara et al. [*Nature Cell Biol.* (2002) 4, 666] and Kuhn and Pollard [*Biohys. J.* (2005) 88, 1387] observed large length fluctuations slightly above  $c_{\text{crit}}$ , provoking speculation that growth may proceed by oligomeric rather than monomeric on-off events. For the single monomer growth process we find that  $D$  exhibits a pronounced peak below  $c_{\text{crit}}$ , due to filaments alternating between capped and uncapped states, a mild version of the dynamic instability of microtubules. Fluctuations just above  $c_{\text{crit}}$  are enhanced but much smaller than those reported experimentally. Future measurements of  $D$  as a function of concentration can help identify the origin of the observed fluctuations.**

The tendency of actin protein to spontaneously polymerize into rapidly growing filaments is fundamental to the life of eukaryotic cells. Cell motility [1, 2], cell division [3], and endocytosis [4] are examples of processes exploiting the dynamic character of actin structures composed of filaments. The regulation of filament growth processes leads to well-defined structures and coordinated function. For example, in combination with branching, capping, and depolymerizing proteins, actin self-assembles into controlled dynamic cross-linked networks forming the dynamic core of lamellipodia [2].

These complex cellular actin-based systems exhibit multiple superposed mechanisms. This has inspired a large body of in vitro work aiming to unravel these mechanisms and pin down rate constants for the constituent processes in purified systems [5]. An important class of experiments entails measuring growth rate at one end by microscopy [6–9] or by bulk spectroscopic methods [10–16] as a function of actin monomer concentration. From these and other in vitro studies using various labeling techniques the following picture has emerged of filament growth kinetics in the presence of ATP (see fig. 1). (i) Monomers are added to a growing filament end as ATP-actin. (ii) Rapidly, the ATP is then hydrolyzed to ADP and phosphate (Pi), both remaining bound to the monomer host (ADP-Pi-actin) [10, 14, 17–22]. A rate of  $0.3\text{s}^{-1}$  was reported in ref. 22 in the presence of Mg, assuming random hydrolysis uninfluenced by neighboring monomers. (iii) After a long delay Pi release into solution occurs, generating ADP-actin [23–25]. Re-

ported release rates are in the range  $0.002 - 0.006\text{s}^{-1}$  [23–26].

A typical filament in a growth rate experiment is thousands of monomer units in length and thus consists mainly of ADP-actin. Hence the picture which emerges is of a long ADP-actin filament with a complex 3-state *cap* region at the filament end [5] (see fig. 1). A major goal of this report is to establish the composition and kinetics of the cap, and how these determine growth rates and measurable length fluctuations. This is important in the context of cellular processes: the monomer composition in actin filaments is thought to regulate actin-binding proteins in a timely and spatially organized way [2]. For example, it has been suggested that rates of branching generated by the Arp2/3 protein complex and/or debranching processes may depend on which of the 3 monomer species is involved, ATP-actin, ADP-Pi-actin or ADP-actin [7, 26, 27]. Pi release has been proposed to act as a timer for the action of the depolymerizing/severing protein ADF/cofilin which preferentially attacks ADP-actin [2].

Our aim in this report is to establish theoretically the quantitative implications of the currently held picture of actin polymerization. Previous theoretical works addressed growth rates before the important process of Pi release was established [28–30]. To date there has been no theoretical analysis of single filament non steady state growth rates rigorously accounting for the processes (i)-(iii) above. A recent theoretical work [31] has addressed steady state filament compositions.

The cap has important consequences for the growth rate  $j$  as a function of ATP-actin concentration,  $c$ . Measured  $j(c)$  curves, such as those in fig. 5, are strikingly non-linear in the region near the concentration where growth rate vanishes [16, 32]. These become almost linear in excess Pi studies, where presumably the ADP-actin species is no longer involved [16]. The complexity of the cap structure and dynamics also underlies the values of the critical concentration  $c_{\text{crit}}$  at the fast-growing “barbed” end and slow-growing “pointed” end of the polar actin filament ( $c_{\text{crit}}$  denotes the concentration where mean growth rate at one end vanishes.) It is well known that in general these are different since detailed balance cannot be invoked for these non-equilibrium polymers [30]. Our work explores how these differences are related to cap structure.

The major experimental focus has been mean growth rates,  $j(c)$ . However, equally revealing are *fluctuations* about the mean whose measurement can expose features of the dynamical processes occurring at filament ends unavailable from  $j(c)$ . These fluctuations are characterized by a “length diffusivity”  $D$  measuring the spread in filament lengths (see fig. 1(b)) similarly to simple one dimensional Fickian diffusion: after time  $t$ , the root mean square fluctuation in filament length is  $(2Dt)^{1/2}$  about the mean value  $j(c)t$ . Using single filament microscopy, Fujiwara et al. [8] and Kuhn and Pollard [9] recently measured unexpectedly high values of this diffusivity near steady state conditions,  $D \sim 30\text{mon}^2/\text{s}$ . This should be compared with what would be expected of an equilibrium polymerization involving the measured on/off rates of order  $1\text{mon}/\text{s}$ , which would lead to  $D \sim 1\text{mon}^2/\text{s}$  [8, 30, 33, 34]. A number of possible explanations were proposed. (i) Fluctua-

\*To whom correspondence should be addressed. E-mail: bo8@columbia.edu

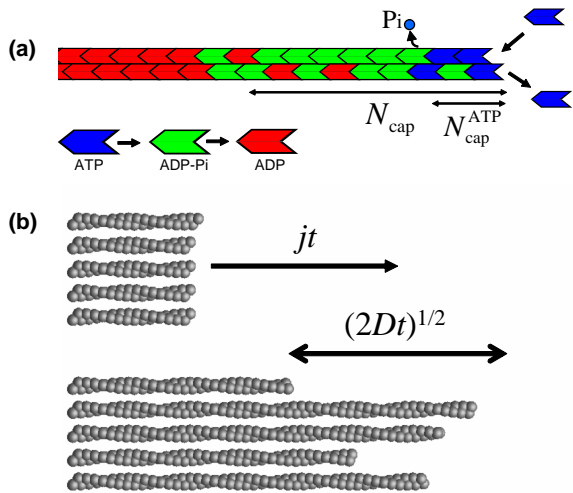


**Figure 1:** (a) Schematic of the 3-species cap at the barbed end of a long actin filament. Near the critical concentration we find a fluctuation-induced cap of  $N_{\text{cap}} \approx 25$  monomers, with a short ATP-actin component,  $N_{\text{cap}}^{\text{ATP}}$  of order one. (b) Mean growth rate and fluctuations: in time  $t$  the average number of monomers added to a filament end is  $jt$ , with a spread of  $(2Dt)^{1/2}$  about this value.

tions arise from “dynamic instability” due to stochastic cap loss episodes. This would be a far milder version of the “catastrophes” in microtubule polymerization [8,35]. (ii) Filament polymerization proceeds by addition and subtraction of *oligomeric* actin segment [8,35]; this would constitute a radical departure from the accepted picture of filament growth kinetics involving single monomer addition events. (iii) Growth involves extra stochastic events such as short pauses possibly originating in filament-surface attachments [9]. (iv) Enhanced fluctuations results from an artifact due to monomer labeling [36]. (v) Experimental error in filament length measurements [9]. A major focus of this report is to calculate the concentration-dependent length diffusivity,  $D(c)$ , assuming that the standard monomer-by-monomer addition picture is valid. We will see that this leads to large  $D$  values *below*  $c_{\text{crit}}$ ; just above the critical concentration fluctuations are enhanced, though much less than the experimental values.

We consider the initial condition where long pre-formed ADP-actin seeds are exposed initially to a buffer of *fixed* actin concentration  $c$  and excess ATP. Thus for a given  $c$  value, a filament consists of a very long ADP-actin core at the end of which lies a complex steady state (but fluctuating) ATP-actin/ADP-Pi-actin cap. Our analysis emphasizes the barbed end, the pointed end assumed blocked. Our results apply to very dilute filaments where only ATP-actin is assumed to add to filaments since (i) free monomers bind ATP more strongly than ADP [37], and (ii) depolymerized ADP-actin or ADP-Pi-actin has enough time to exchange its nucleotide for ATP before repolymerization. An important issue is the nature of the ATP hydrolysis mechanism: the experiments of refs. 20, 21 support a random mechanism, though others have suggested a cooperative vectorial mechanism occurring at the interface between ADP-Pi-actin and ATP-actin with rate  $13.6\text{s}^{-1}$  [19,28]. In this study, random hydrolysis is assumed throughout.

## Parameter Values and Mathematical Methods

One of the major aims of this work is to identify qualitative, but experimentally measurable, features of the growth kinet-

ics which are independent of the precise values of rate constants, since the latter depend on experimental conditions such as ionic strength [38] and the values themselves are often controversial. The parameter values we use are shown in table 1 in which  $k_{\text{T}}^+$  is the polymerization rate constant of ATP-actin, and  $v_{\text{T}}^-$ ,  $v_{\text{D}}^-$  and  $v_{\text{P}}^-$  are the depolymerization rates of ATP-actin, ADP-actin, and ADP-Pi-actin, respectively. The rates of ATP-hydrolysis and Pi release (both assumed irreversible) are  $r_{\text{H}}$  and  $r_{\text{Pi}}$ , respectively. In addition, we will explore the effects of changing some of these parameter values. Since the monomer at the tip makes bonds with two nearest neighbors, each belonging to a different protofilament, one expects that rate constants may also depend on the state of neighbors. Here, however, we study the simplest “one body” model, assuming on/off rates depend only on the attaching/detaching species [6] and that hydrolysis and Pi release rates are uniform along the filament. The influence of “many body” effects will be briefly discussed below.

To calculate filament growth kinetics and composition one is faced with the formidable task of obtaining the steady state probability distribution of all possible actin monomer sequences along the filament: there are 3 possible states per monomer, so for filaments of  $N$  units long this necessitates solving  $3^N$  coupled equations. We have managed, however, to obtain a solution for the mean elongation rate  $j(c)$  by projecting the full system of  $3^N$  equations onto a set of just 3 exact equations for the return probabilities  $\psi_{\text{T}}^{\text{A}}$ ,  $\psi_{\text{T}}^{\text{P}}$ , and  $\psi_{\text{T}}^{\text{D}}$ . These are the probabilities that a given monomer which was polymerized at  $t = 0$  is again at the tip at time  $t$  as ATP-actin, ADP-Pi-actin, or ADP-actin, respectively.

The outline of our method is as follows. For  $j < 0$  the growth rate is related to the return probabilities by  $j = v_{\text{D}}^- p_{\text{core}}$ , where  $p_{\text{core}} = 1 - \int_0^{\infty} dt (\psi_{\text{T}}^{\text{D}} + \psi_{\text{T}}^{\text{P}} + \psi_{\text{T}}^{\text{A}})$  is the probability of exposure of the ADP-actin core at the tip. For  $j > 0$ , the relation is  $j = k_{\text{T}}^+ c - \int_0^{\infty} dt F_t$  where  $F_t \equiv \psi_{\text{T}}^{\text{A}} v_{\text{T}}^- + \psi_{\text{T}}^{\text{P}} v_{\text{P}}^- + \psi_{\text{T}}^{\text{D}} v_{\text{D}}^-$  is the mean depolymerization rate at time  $t$  of a monomer which added to the tip at  $t = 0$ . The integral of  $F_t$  is the total depolymerization rate of added monomers. In the supporting material we present the dynamical equations obeyed by the return probabilities, from which we obtained a closed recursion relation for the Laplace transform of  $F_t$ , namely  $f_E$ . This relates  $f_E$  to  $f_{E+r_{\text{H}}}$  and  $f_{E+r_{\text{Pi}}}$ . With boundary condition  $f_E \rightarrow 0$  as  $E \rightarrow \infty$ , we started from large  $E$  values and evolved this equation numerically towards  $E = 0$  to obtain  $f_0 \equiv \int_0^{\infty} dt F_t$ . Given  $f_0$ , the time integrals of the return probabilities were then directly obtained from the dynamical equations and  $j$  was thereby determined.

The above analytically based method does not generate cap sizes and length diffusivities. In order to calculate these quantities and also to test the validity of the analytical method we have simulated the stochastic tip dynamics employing the kinetic Monte Carlo (MC) method known as the BKL [39] or Gillespie [40] algorithm, to evolve the state of a filament tip in time and to calculate its mean growth rate. Each step of the algorithm entails updating time by an amount depending on the rate and number of possible future events, namely polymerization/depolymerization, hydrolysis, and Pi release. Excellent agreement is found between MC results and the numerical solutions of our closed equations for the growth rate (see inset of fig. 3).

Our analytical method is exact and avoids preaveraging, an approximation where the joint probability of a given filament nucleotide sequence is approximated as a product of probabilities for individual actin subunits. This neglects correlations between units. To assess the accuracy of this scheme, we compared our results for cap size and growth rate to those obtained using preaveraging (see supporting material for details). Preav-

$k_T^+$ ( $\mu\text{M}^{-1}\text{s}^{-1}$ )	$v_T^-$	$v_P^-$	$v_D^-$	$r_H$	$r_{\text{Pi}}$
11.6 <sup>(a)</sup>	1.4 <sup>(a)</sup>	1.1 <sup>(b)</sup>	7.2 <sup>(a)</sup>	0.3 <sup>(c)</sup>	0.004 <sup>(d)</sup>

Table 1: Values of barbed end rate constants used in this work, appropriate for solutions of 50mM KCl and 1mM MgCl<sub>2</sub>. Units in s<sup>-1</sup> unless otherwise indicated. <sup>(a)</sup> From ref. [6]. <sup>(b)</sup> Assigned; at present there is no direct measurement of  $v_P^-$ , but  $j(c)$  measurements with excess Pi [16] show the sum of the ADP-Pi-actin off rates at both ends together is a few times smaller than  $v_D^-$ . <sup>(c)</sup> From ref. [22]. <sup>(d)</sup> From refs. [23–26].

eraging has been used in other theoretical studies of actin polymerization such as ref. [31] to study steady state and ref. [32] to study growth rates.

## Cap Structure and the Importance of Fluctuations

Using the parameters of table 1, in fig. 2 we present MC results for (i) the total cap size,  $N_{\text{cap}}$ , namely the mean total number of ATP-actin and ADP-Pi-actin subunits at the barbed end, as a function of concentration, and (ii) the number of ATP-actin cap subunits,  $N_{\text{cap}}^{\text{ATP}}$ . The figure shows that both caps become large for large concentrations. This is easy to understand. Consider for example the ATP cap: when polymerization rates exceed both the hydrolysis rate  $r_H$  and the depolymerization rates, the interface between ADP-Pi-actin and ATP-actin follows the growing tip with a lag of  $j(c)/r_H$  monomers. Thus

$$N_{\text{cap}}^{\text{ATP}} = j(c)/r_H, \quad N_{\text{cap}}^{\text{ADPPi}} = j(c)/r_{\text{Pi}} \quad (c \gg c_{\text{crit}}) \quad (1)$$

Here the number of ADP-Pi subunits,  $N_{\text{cap}}^{\text{ADPPi}}$ , is found using similar reasoning as for  $N_{\text{cap}}^{\text{ATP}}$ . The validity of eq. (1) for large concentrations is verified against MC data in fig. 2.

The striking feature of fig. 2 is that the total cap remains long even *below* the critical concentration of the barbed end, being 25 units at  $c_{\text{crit}}$  and remaining larger than unity down to  $c \approx c_{\text{crit}}/2$ . One might naively have guessed that below  $c_{\text{crit}}$  there would be no cap at all, since the filament is shrinking into its ADP core. (Indeed, the absence of a cap would also be suggested by eq. (1) if one were to extend its validity down to  $c_{\text{crit}}$  where  $j = 0$ .) This reasoning is however invalid because it neglects fluctuations due to randomness of monomer addition/subtraction.

To understand why fluctuations lead to long caps, consider the length changes of the cap only, excluding changes in the ADP-actin core length. Just below the critical concentration the tip of a typical long cap has a net shrinkage rate  $v_{\text{cap}}(c)$ . This is a weighted average of rates, summed over all possible states of the short ATP-actin segment on top of the long ADP-Pi-actin segment. Since  $v_{\text{cap}}$  is a smooth function of  $c$ , it can be Taylor-expanded near the critical concentration and expressed as  $v_{\text{cap}} = k_{\text{eff}}^+(c - c_{\text{crit}})$  where  $k_{\text{eff}}^+$  is an effective on rate constant, different from  $k_T^+$ . Now superposed on this average shrinkage the cap tip also performs a random walk in cap length space, described by a diffusivity  $D_{\text{cap}}(c)$  [8,33,34], also an average over the states of the short ATP cap. ( $D_{\text{cap}}$  is in fact the *short-time* diffusivity of the entire filament, see discussion below.) For small times, diffusivity dominates and of order  $(2D_{\text{cap}}t)^{1/2}$  units add to or subtract from the cap. For times less than the cap turnover time  $t_{\text{cap}}$ , this is much bigger than the number of units wiped out by coherent shrinkage,  $v_{\text{cap}}t$ . The cap lifetime  $t_{\text{cap}}$  is the time when the shrinkage just catches up,  $v_{\text{cap}}t_{\text{cap}} \approx (2D_{\text{cap}}t_{\text{cap}})^{1/2}$ . Hence the approxi-

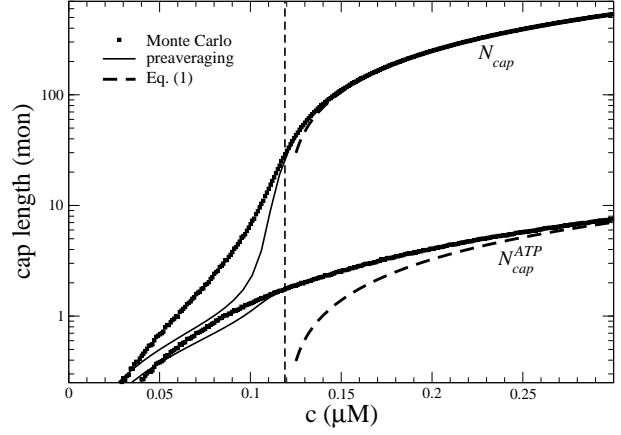


Figure 2: Total cap length  $N_{\text{cap}}(c)$  and ATP-actin cap length  $N_{\text{cap}}^{\text{ATP}}(c)$  at barbed end. Parameters from table 1. Squares: MC results. Dashed lines: eq. (1). Solid lines: preaveraging approximation. Vertical dashed line indicates  $c_{\text{crit}} = 0.119\mu\text{M}$ .

mate dependence of cap length on concentration is

$$N_{\text{cap}} = v_{\text{cap}}t_{\text{cap}} \approx 2D_{\text{cap}}/[k_{\text{eff}}^+(c_{\text{crit}} - c)], \quad (c < c_{\text{crit}}) \quad (2)$$

which indeed becomes large as  $c_{\text{crit}}$  is approached from below.

In summary, even though *on average* below  $c_{\text{crit}}$  no ATP-actin monomers are being added to the tip, *fluctuations* in addition/subtraction rates allow a cap to grow to length  $(2D_{\text{cap}}t_{\text{cap}})^{1/2}$  because the cap length diffusivity is dominant for times less than  $t_{\text{cap}}$ . Now since Pi release is very slow, for simplicity in deriving eq. (2) we assumed the release rate was zero,  $r_{\text{Pi}} = 0$ . However, the result of eq. (2) is valid even for a non-zero  $r_{\text{Pi}}$  except for concentrations so close to  $c_{\text{crit}}$  that the cap turnover time exceeds the Pi release time. In this inner region, diffusion is only able to grow the cap for a time of order  $r_{\text{Pi}}^{-1}$  before Pi release intervenes. The maximum possible cap length, attained very close to  $c_{\text{crit}}$ , is thus

$$N_{\text{cap}}^{\text{crit}} \approx [2D_{\text{cap}}(c_{\text{crit}})/r_{\text{Pi}}]^{1/2} \quad (3)$$

Eq. (2) is valid until  $N_{\text{cap}}$  reaches this bound.

These arguments explain the origin of the long caps below  $c_{\text{crit}}$ . To make quantitative comparison of eqs. (2) and (3) to the numerics of fig. 2, the values of  $D_{\text{cap}}$  and  $v_{\text{cap}}$  must be determined. Now since for our parameter set  $v_T^-$  and  $v_P^-$  have similar values (see table 1), an estimate can be obtained by considering the special case where  $v_T^- = v_P^-$  (identical ATP-actin and ADP-Pi-actin). This is a convenient case because  $D_{\text{cap}}$  and  $v_{\text{cap}}$  can be calculated exactly; the cap has just one monomer species, so  $k_{\text{eff}}^+ = k_T^+$ , and  $D_{\text{cap}}(c_{\text{crit}}) = (k_T^+c_{\text{crit}} + v_T^-)/2$  [8,33,34]. Using the values of table 1 in these expressions and in eq. (3) gives  $N_{\text{cap}}^{\text{crit}} \approx 26$ , of the same order as the numerics of fig. 2.

Finally, note that the preaveraging method shown in fig. 2 is an excellent approximation in regions where fluctuations are unimportant (very large or very small  $c$ ), producing almost identical results to MC. However, below  $c_{\text{crit}}$  it considerably underestimates cap lengths. This results from the preaveraged treatment of fluctuations.

## Mean Growth Rate, $j(c)$

How is the behavior of the average rate of growth  $j(c)$  correlated to cap structure and dynamics? The lowest curve of

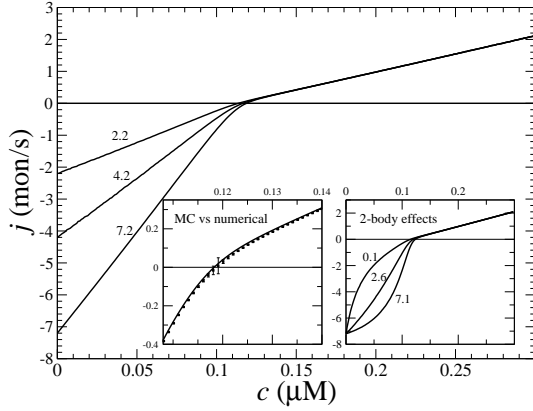


Figure 3: Dependence of growth rate on concentration; Influence of  $v_D^-$  (indicated in  $s^{-1}$  next to each curve). Other parameters as in table 1. MC and exact numerical solution results are indistinguishable. The spread in  $c_{crit}$  values for the 3 curves is 5%. Left inset: blow up of critical region showing the agreement between MC (squares, error bars are standard deviation of mean) and numerical method (solid line). Right inset: Influence of many body effects; the value shown in  $s^{-1}$  next to curves is depolymerization rate of ATP-actin next to ADP-actin,  $v_{TD}^-$ .

fig. 3 shows numerical results for barbed end growth, using identical parameters to those of fig. 2. A noticeable feature is that the slopes are very different above and below the critical concentration of the barbed end. This directly reflects the cap structure just discussed, as follows. For  $c \gg c_{crit}$  the ATP-actin segment is long and hides the remaining ADP-Pi-actin portion of the cap, so  $j \approx k_T^+ c - v_T^-$  has simple linear form and slope  $k_T^+$ , approximately behaving as if ATP-actin were the only species involved. On the other hand for  $c < c_{crit}$ , the slope of  $j(c)$  is large because the cap length is changing rapidly as concentration increases (see fig. 2). Filament length change is now generated by capless episodes, when the ADP-actin core is exposed and the filament shrinks with velocity  $v_D^-$  (the steady state cap has fixed mean length and does not on average contribute). Thus  $j = -v_D^- p_{core}$  where  $p_{core} \approx 1/N_{cap}$  is the probability the cap length vanishes, assuming a broad distribution of cap lengths with mean  $N_{cap}$ . Using eq. (2), this gives  $j \approx v_D^- k_{eff}^+ (c_{crit} - c)/(2D_{cap})$  in the region where eq. (2) is valid. Since  $v_D^-$  is large, this is a much larger slope than for concentrations above  $c_{crit}$ .

The region very close to  $c_{crit}$ , where eq. (3) takes over, is an interesting one: (1) Here the total cap becomes long, of length approximately  $N_{cap}^{crit}$ , implying that ADP-actin is rarely exposed at the tip. This in turn implies that the depolymerization rate of ADP-actin will have only a small influence on the value of  $c_{crit}$ . This is verified in fig. 3 where we display  $j(c)$  curves for  $v_D^-$  values ranging from 2.2 to  $7.2s^{-1}$ . These changes produce only a very small shift in  $c_{crit}$ , even though  $j(c)$  changes significantly for  $c < c_{crit}$ . (2) The mean ATP-cap length is small (of order unity), and since the tip composition and cap length is constantly fluctuating, both ATP-actin and ADP-Pi-actin are frequently exposed at the tip. Thus we expect a dependence of  $c_{crit}$  on the value of  $v_P^-$ . This is verified in fig. 4 where we display how the growth rate and  $c_{crit}$  change with the value of  $v_P^-$ . The magnitude of the shift is influenced by the assumed rate of ATP hydrolysis: if one uses, for example, a hydrolysis rate 10 times smaller, the change in growth remains substantial but is considerably reduced (see inset).

Note also that preaveraging estimates the growth rate very accurately (see fig. 4). Even in the fluctuation-dominated re-

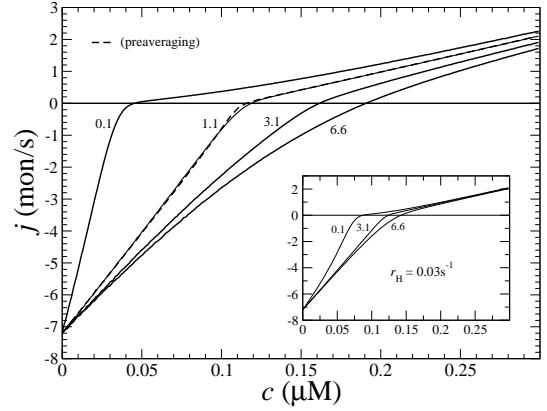


Figure 4: Growth rate: influence of the value of  $v_P^-$  (shown in  $s^{-1}$ ). Other values as in table 1. Solid lines: numerical solutions and MC simulations (indistinguishable). Dashed line: preaveraging approximation for  $v_P^- = 1.1s^{-1}$ . Inset: same but with  $r_H = 0.03s^{-1}$ .

gion just below  $c_{crit}$ , where cap size is substantially underestimated, it remains accurate though slightly less so than elsewhere.

An important question is the effect of many body interactions between actin subunits, so far neglected in this report. We have found that the shape of the mean growth rate near and below the critical concentration is sensitive to these. As an example, fig. 3 (inset) shows the dependence of  $j(c)$  on the depolymerization rate of ATP-actin when its nearest neighbor is ADP-actin ( $v_{TD}^-$ ), with all other rates as in table 1. Other types of many body interactions can lead also to shifts in  $c_{crit}$  (not shown). Including many body interactions rapidly increases the number of rate constants. Since these are unknown and presumably hard to measure, this limits the uniqueness with which growth rate curves can be modeled near  $c_{crit}$ . We stress, however, that the central qualitative conclusions, namely the existence of a long cap at  $c_{crit}$  and the associated change of slope of the growth rate, are general. An example of fitting experimental  $j(c)$  curves with a one body model is shown in fig. 5.

## Fluctuations in Growth Rate

Turning now to fluctuations in growth rates, we find these behave dramatically around the critical concentration reflecting a mild version of the dynamic instability exhibited by microtubules [30, 41]. In the inset of fig. 6 we used MC to evaluate the length diffusivity,  $D(t) \equiv (\langle L^2 \rangle - \langle L \rangle^2)/(2t)$ , where  $L$  is the number of subunits added/subtracted after time  $t$ , starting from filaments with steady state caps at  $t = 0$ . For  $c = 0.15\mu M$  (above  $c_{crit}$ ) we find  $D$  is essentially independent of time. Its magnitude is of order  $1\text{mon}^2/\text{s}$ , as would be expected for a growth process of identical subunits which add/subtract with rates of order  $1s^{-1}$  [8, 30, 33, 34]. However, for  $c = 0.1\mu M$  (below  $c_{crit}$ )  $D$  is increasing with time, reaching a large asymptotic value  $D_\infty$  after several hundred seconds. Fig. 6 shows the dependence of  $D_\infty$  on concentration; it exhibits a sharp peak below  $c_{crit}$  and then drops rapidly.

To understand the physics underlying this behavior, consider the simple model where ATP-actin and ADP-Pi-actin are identical ( $v_T^- = v_P^-$ ) and Pi release very slow ( $r_{P_i} \rightarrow 0$ ). Now  $D$  describes the random walk performed by the filament tip; if the tip makes a random forwards or backwards step of  $L$  monomer units every time interval  $T$ , then one can write

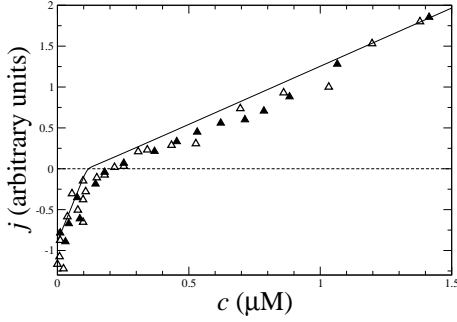


Figure 5: Growth rate  $j(c)$  versus concentration from data taken from fig. 1 of ref. 14 for simultaneous growth at both ends (in KCl and Mg). Solid line: numerical results, barbed end (parameters from table 1), multiplied by a prefactor to fit data which lack absolute scale. Differences between numerical and experimental results may originate from the pointed end contribution, or possibly due to the experimental ionic conditions.

$D = L^2/T$ . Just above the critical concentration, where on and off rates are approximately equal, the tip randomly adds or subtracts one ATP-actin ( $L = 1$ ) in a mean time  $T = 1/v_T^-$ , giving  $D = v_T^-$ . Just below the critical concentration, however, we know there is a long steady state cap. Since most filaments are capped, at short times  $D$  is determined by length changes of the cap and its value is thus close to the cap diffusivity,  $D_{\text{cap}}$ . As time increases, more and more uncapping episodes occur, each episode now contributing to filament length change. Such events are correlated on the timescale of the cap lifetime,  $t_{\text{cap}} \approx N_{\text{cap}}^2/v_T^-$  (we used  $D_{\text{cap}} = v_T^-$  for the simple model [33, 34].) This explains why  $D(t)$  changes with time up to the cap lifetime (see fig. 6, inset). Thus to determine  $D_\infty$ , one must take  $T = t_{\text{cap}}$ . Using a well known result from the theory of 1D random walks [42], the number of uncapping events during the time  $t_{\text{cap}}$  is approximately  $(D_{\text{cap}}t_{\text{cap}})^{1/2} \approx N_{\text{cap}}$ . Since the number of core monomers lost during each uncapping episode before a polymerizing monomer arrives is of order  $v_D^-/v_T^-$ , thus  $L = N_{\text{cap}}v_D^-/v_T^-$ . This leads to a very different expression for the diffusivity,  $D_\infty \approx (v_D^-)^2/v_T^-$ : there is a discontinuity in diffusivity at  $c_{\text{crit}}$  of magnitude

$$\Delta D_\infty = v_T^-(\lambda^2 - 1), \quad \lambda \equiv v_D^-/v_T^-. \quad (4)$$

At the barbed end the instability parameter  $\lambda \approx 5.1$  and fluctuations at the critical concentration are very large, with a pronounced discontinuous drop in  $D_\infty$  as one passes to higher  $c$ . A rigorous derivation of eq. (4) is shown in the supporting material where in addition we obtain the full sawtooth curve shown in fig. 6; evidently, the simple model captures many features of the actual  $D_\infty(c)$  profile. The effect of Pi release and ATP-actin/ADP-Pi-actin differences is to shift  $c_{\text{crit}}$  and to smooth the sharp peak and shift it to somewhat below  $c_{\text{crit}}$ .

How do the results of fig. 6 compare to the large fluctuations observed by Fujiwara et al. [8] and Kuhn and Polard [9], and also suggested by the findings of ref. 43? Fig. 6 shows a peak value of  $D_\infty \approx 34 \text{mon}^2 \text{s}^{-1}$ , dropping to  $D_\infty \approx 5 \text{mon}^2 \text{s}^{-1}$  at  $c_{\text{crit}}$ . The experimentally reported value was  $\sim 30 \text{mon}^2 \text{s}^{-1}$ ; however, these measurements were performed at [8] or close [9] to a treadmilling steady state, i. e. at a concentration slightly above  $c_{\text{crit}}$  for the barbed end and well below that for the pointed end. At this concentration, fig. 6 shows a diffusivity less than  $5 \text{mon}^2 \text{s}^{-1}$ . Thus both theory and experiment exhibit large fluctuations near  $c_{\text{crit}}$ , but at different concentrations. Future experimental measurements of the full  $D_\infty(c)$  profile are needed to establish the relationship, if any, between these.

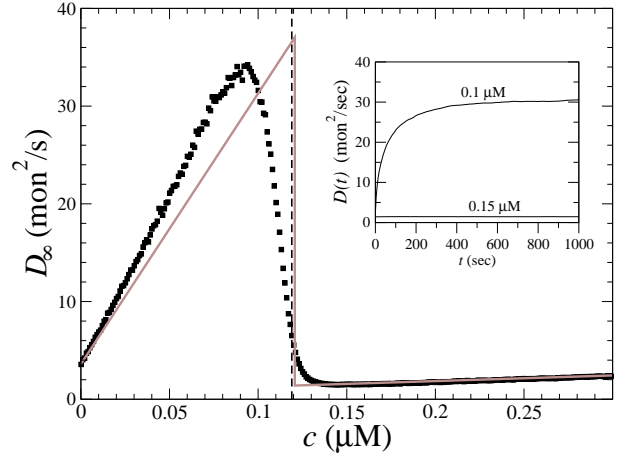


Figure 6: Long time length diffusion coefficient,  $D_\infty(c)$ . Squares: MC results, parameters from table 1. Vertical dashed line indicates  $c_{\text{crit}}$ . Solid line: prediction of simple model:  $v_P^- = v_T^- = 1.4 \text{s}^{-1}$ ,  $r_{\text{Pi}} = 0$ , other values from table 1. Inset: Time-dependence of diffusivity at two concentrations.

Our work leads also to the following prediction: since phosphate will bind to ADP-actin and eliminate the effect of a large instability parameter, thus fluctuations and  $D$  at the barbed end will be suppressed in the presence of excess Pi.

## Discussion

**Pointed End  $j(c)$ : Why is  $c_{\text{crit}}$  so Different?** In this study we emphasized the barbed end, but our methods are also applicable to the pointed end, provided the same mechanisms of uniform random hydrolysis and slow Pi release remain valid. Making this assumption, let us now discuss why  $c_{\text{crit}}$  (for ATP-actin) at the pointed end is almost six times the value at the barbed end [6]. Now an important issue is how different the ATP-actin and ADP-Pi-actin species are, in terms of on and off rate constants. That they are similar is suggested by the observation that excess phosphate reduces the critical concentration in a pure ADP-actin polymerization to a value rather close to the barbed end  $c_{\text{crit}}$  in ATP [16, 44, 45]. But if indeed the 2 species are similar, and the same basic mechanisms apply at the pointed end, this is inconsistent with the very different  $c_{\text{crit}}$  values. This inconsistency is due to the cap structure we have established here: the cap includes a long ADP-Pi segment essentially *hiding* the ADP-actin core which is thus *rarely seen* at the filament tip (see fig. 1(a)). For the barbed end (fig. 2)  $N_{\text{cap}} \approx 25$  at  $c_{\text{crit}}$ , and we find a large value for the pointed end at its  $c_{\text{crit}}$ , though smaller than the barbed end (data not shown). Thus ADP-actin on/off rates are almost irrelevant to  $c_{\text{crit}}$  (see fig. 3) and hence differences between ATP-actin and ADP-actin cannot account for the large  $c_{\text{crit}}$  differences. Thus the origin must be different ATP-actin/ADP-Pi-actin compositions at the pointed and barbed ends; since the ATP-actin segment is short both species are regularly exposed at filament ends and substantially different  $c_{\text{crit}}$  values will result provided the 2 species have different rate constants. Were these identical,  $c_{\text{crit}}$  at both ends would be very similar, because the on/off rates at the filament ends would then be very close to the values for an all ATP-actin filament; for such a filament, detailed balance dictates that the ratio of on/off rates at each end are identical [30]. (However, in apparent contradiction to this conclusion are the findings of ref. [6] where different on/off ratios were reported at each end, under conditions where long ATP-actin caps are expected. A conceivable explanation is possibility (ii), see below.) Many body effects will further affect  $c_{\text{crit}}$ .



We are driven to two possibilities: (i) ATP-actin and ADP-Pi-actin are substantially different, or (ii) different mechanisms operate during pointed end growth. Certain workers [46, 47] have proposed possibility (i), based on the irreversibility of hydrolysis [46] which suggests a large energetic change, possibly a structural change of the filament. Possibility (i) may in fact be consistent with the experiments of refs. 16, 44, 45 which did not probe individual on/off rate constants of ADP-Pi-actin and which may have involved significant ADP-actin polymerization [45]. We are unaware of any crystallographic [48] or electron microscopic [49] experiments examining ATP/ADP-Pi differences for filamentous actin.

If we adhere to the assumption that the growth mechanisms as previously outlined apply to both ends, we are then led to the following prediction: the values of  $c_{\text{crit}}$  for ATP-actin at both ends will be only weakly affected by the presence of excess Pi (provided ionic conditions are strictly unchanged). This is because the binding of Pi to ADP-actin segments is almost irrelevant since these are rarely exposed at the tip due to long caps at  $c_{\text{crit}}$ . Indeed, for the barbed end no significant shift has been observed in the presence of Pi [16, 44, 45]. For the pointed end, however, a reduction of  $c_{\text{crit}}$  has been reported in the presence of Pi and barbed end capping proteins [16, 44, 45]. This cannot be explained within the present framework and suggests possibility (ii). Future experiment will hopefully settle this important issue.

**Conclusions.** In this work filament growth rates  $j(c)$  and their fluctuations, as measured by the diffusivity  $D(c)$ , were calculated as functions of ATP-actin concentration  $c$ . To our knowledge, this is the first rigorous calculation of these quantities accounting for all known basic mechanisms. Pantaloni et al. [28, 29] studied  $j(c)$  at the barbed end in a work before the mechanism of Pi release was discovered. Infinitely fast Pi release and vectorial hydrolysis were assumed. Given the data available at that time, in order to explain the sharp change in slope of  $j(c)$  at  $c_{\text{crit}}$  (see e.g. fig. 5), they further assumed (i) strong three body ATP-actin/ADP-actin interactions which lead to stable short ATP-actin caps, and (ii) zero hydrolysis rate of the nucleotide bound to the terminal monomer. In our work, the origin of the sharp change in slope is precisely the fact that Pi release is slow, similarly to an earlier model of microtubule polymerization [50].

Recently, Bindschadler et al. [31] studied the composition of actin filaments accounting for all three actin species at steady state. We have examined the preaveraging approximation used in their work and showed that it leads to very accurate  $j(c)$  curves, but the cap lengths are underestimated below  $c_{\text{crit}}$ .

Here we have addressed random ATP hydrolysis only. Future work is needed to analyze the implications of the vectorial hydrolysis suggested by refs. 19, 28. We showed that for random hydrolysis  $j(c)$  is linear far above the critical concentration. Growth rate experiments for both ends together in the absence of KCl have exhibited non-linearities up to  $c = 10\mu\text{M}$ , far above the critical concentration of the barbed end which is  $1\mu\text{M}$  under these conditions [10, 11]. In refs. 10, 28 this observation was attributed to vectorial hydrolysis at the barbed end while in ref. 6 this was assigned to the non-linear contribution of the pointed end whose critical concentration is  $\approx 5\mu\text{M}$  under the same conditions.

Perhaps our most interesting finding is that the long time diffusivity  $D_{\infty}$  has a large peak below the critical concentration  $c_{\text{crit}}$  of the barbed end, followed by a sharp drop in a narrow range above  $c_{\text{crit}}$ . This conclusion is quite general and its origin is the smallness of the Pi release rate and the large value of the off rate of ADP-actin at the barbed end. Future measurements of length diffusivities over a range of concentrations promise to provide new information and insight on the fundamentals of actin polymerization.

This work was supported by the Petroleum Research Fund, grant 33944-AC7, and NSF, grant CHE-00-91460. We thank Ikuko Fujiwara, Jeffrey Kuhn and Thomas Pollard for stimulating discussions.

## References

- [1] Bray, D. (2000) *Cell Movements. From Molecules to Motility*, 2nd Ed. (Garland Publishing, New York).
- [2] Pollard, T. D & Borisy, G. G. (2003) *Cell* **112**, 453–465.
- [3] Pelham, R. J & Chang, F. (2002) *Nature* **419**, 82–86.
- [4] Young, M. E, Cooper, J. A, & Bridgman, P. C. (2004) *J. Cell. Biol.* **166**, 629–635.
- [5] Korn, E. D, Carlier, M.-F, & Pantaloni, D. (1987) *Science* **238**, 638–643.
- [6] Pollard, T. D. (1986) *J. Cell Biol.* **103**, 2747–2754.
- [7] Amann, K. J & Pollard, T. D. (2001) *Proc. Natl. Acad. Sci. USA* **98**, 15009–15013.
- [8] Fujiwara, I, Takahashi, S, Takaduma, H, Funatsu, T, & Ishiwata, S. (2002) *Nature Cell Biology* **4**, 666–673.
- [9] Kuhn, J & Pollard, T. D. (2005) *Biophys. J.* **88**, 1387–1402.
- [10] Carlier, M.-F, Pantaloni, D, & Korn, E. D. (1984) *J. Biol. Chem.* **259**, 9983–9986.
- [11] Carlier, M.-F, Pantaloni, D, & Korn, E. D. (1985) *J. Biol. Chem.* **260**, 6565–6571.
- [12] Coué, M & Korn, E. D. (1986) *J. Biol. Chem.* **261**, 1588–1593.
- [13] Carlier, M.-F, Crique, P, Pantaloni, D, & Korn, E. D. (1986) *J. Biol. Chem.* **261**, 2041–2050.
- [14] Carlier, M.-F, Pantaloni, D, & Korn, E. D. (1986) *J. Biol. Chem.* **261**, 10785–10792.
- [15] Weber, A, Northrop, J, Bishop, M. F, Ferrone, F. A, & Mooseker, M. S. (1987) *Biochemistry* **26**, 2537–2544.
- [16] Carlier, M.-F & Pantaloni, D. (1988) *J. Biol. Chem.* **263**, 817–825.
- [17] Pardee, J. D & Spudich, J. A. (1982) *J. Cell Biol.* **93**, 648–654.
- [18] Pollard, T. D & Weeds, A. G. (1984) *FEBS Lett.* **170**, 94–98.
- [19] Carlier, M.-F, Pantaloni, D, & Korn, E. D. (1987) *J. Biol. Chem.* **262**, 3052–3059.
- [20] Ohm, T & Wegner, A. (1994) *Biochim. Biophys. Acta* **1208**, 8–14.
- [21] Pieper, U & Wegner, A. (1996) *Biochemistry* **35**, 4396–4402.
- [22] Blanchoin, L & Pollard, T. D. (2002) *Biochemistry* **41**, 597–602.
- [23] Carlier, M.-F & Pantaloni, D. (1986) *Biochemistry* **35**, 7789–7792.
- [24] Carlier, M.-F. (1987) *Biochemical and Biophysical Research Communications* **143**, 1069–1075.
- [25] Melki, R, Fievez, S, & Carlier, M.-F. (1996) *Biochemistry* **35**, 12038–12045.
- [26] Blanchoin, L, Pollard, T. D, & Mullins, R. D. (2000) *Curr. Biol.* **10**, 1273–1282.
- [27] Ichetovkin, I, Grant, W, & Condeelis, J. (2002) *Curr. Biol.* **12**, 79–84.
- [28] Pantaloni, D, Hill, T. L, Carlier, M. F, & Korn, E. D. (1985) *Proc. Natl. Acad. Sci. USA* **82**, 7207–7211.
- [29] Hill, T. L. (1986) *Biophys. J.* **49**, 981–986.
- [30] Hill, T. L. (1987) *Linear Aggregation Theory in Cell Biology*. (Springer Verlag, New York).
- [31] Bindschadler, M, Osborn, E. A, Dewey, C. F. J, & McGrath, J. L. (2004) *Biophys. J.* **86**, 2720–2739.
- [32] Keiser, T, Schiller, A, & Wegner, A. (1986) *Biochemistry* **25**, 4899–4906.
- [33] O’Shaughnessy, B & Vavylonis, D. (2003) *Phys. Rev. Lett.* **90**, 118301.
- [34] O’Shaughnessy, B & Vavylonis, D. (2003) *Eur. Phys. J. E* **12**, 481–496.
- [35] Littlefield, R & Fowler, V. M. (2002) *Nature Cell Biology* **4**, E209–E210.
- [36] Kudryasov, D. S, Phillips, M, & Reisler, E. (2004) *Biophys. J.* **87**, 1136–1145.
- [37] Kinosian, H. J, Selden, L. A, Estes, J. E, & Gershman, L. C. (1993) *J. Biol. Chem.* **268**, 8683–8691.
- [38] Drenckhahn, D & Pollard, T. D. (1986) *J. Biol. Chem.* **261**, 12754–12758.
- [39] Bortz, A. B, Kalos, M. H, & Lebowitz, J. L. (1975) *Journal of Computational Physics* **17**, 10–18.
- [40] Gillespie, D. T. (1977) *J. Phys. Chem.* **81**, 2340–2361.
- [41] Hill, T. L & Chen, Y.-D. (1984) *Proc. Natl. Acad. Sci. USA* **81**, 5772–5776.
- [42] Fisher, M. E. (1984) *J. Stat. Phys.* **34**, 667–729.
- [43] Brenner, S. L & Korn, E. D. (1983) *J. Biol. Chem.* **258**, 5013–5020.
- [44] Rickard, J. E & Sheterline, P. (1986) *J. Mol. Biol.* **191**, 273–280.
- [45] Wanger, M & Wegner, A. (1987) *Biochimica et Biophysica Acta* **915**, 105–113.
- [46] Carlier, M.-F, Pantaloni, D, Evans, J. A, Lambooy, P. K, Korn, E. D, & Webb, M. R. (1988) *FEBS Letters* **235**, 211–214.
- [47] Dickinson, R. B, Caro, L, & Purich, D. L. (2004) *Biophys. J.* **87**, 2838–2854.
- [48] Otterbein, L. R, Graceffa, P, & Dominguez, R. (2001) *Science* **293**, 708–711.
- [49] Belmont, L. D, Orlova, A, Drubin, D. G, & Egelman, E. H. (1999) *Proc. Natl. Acad. Sci. USA* **96**, 29–34.
- [50] Hill, T. L & Carlier, M.-F. (1983) *Proc. Natl. Acad. Sci. USA* **80**, 7234–7238.

# SUPPORTING MATERIAL

## A. Numerical Method for Growth Rates.

In this part of the supporting material we describe the numerical method we used in the main text to calculate the growth rate curves of figs. 3 and 4. Consider an ATP-actin monomer which polymerizes at the filament tip at time  $t = 0$ . We define the return probabilities  $\psi_t^T$ ,  $\psi_t^P$ , and  $\psi_t^D$  to be the probability that this monomer is once again at the tip after time  $t$  as ATP-actin, ADP-Pi-actin, or ADP-actin, respectively. The total depolymerization rate of this monomer at time  $t$  is

$$F_t = v_T^- \psi_t^T + v_P^- \psi_t^P + v_D^- \psi_t^D . \quad (5)$$

The dynamical equations obeyed by the return probabilities are

$$\begin{aligned} \frac{d}{dt} \psi_t^T &= -(k_T^+ c + v_T^- + r_H) \psi_t^T + k_T^+ c \int_0^t dt' \psi_{t-t'}^T F_{t-t'} e^{-r_H(t-t')} , \\ \frac{d}{dt} \psi_t^P &= -(k_T^+ c + v_P^- + r_{Pi}) \psi_t^P + r_H \psi_t^T + k_T^+ c \int_0^t dt' \psi_{t-t'}^P F_{t-t'} e^{-r_{Pi}(t-t')} \\ &\quad + k_T^+ c \int_0^t dt' \psi_{t-t'}^T F_{t-t'} \frac{r_H}{r_{Pi} - r_H} \left( e^{-r_H(t-t')} - e^{-r_{Pi}(t-t')} \right) , \\ \frac{d}{dt} \psi_t^D &= -(k_T^+ c + v_D^-) \psi_t^D + r_{Pi} \psi_t^P + k_T^+ c \int_0^t dt' \psi_{t-t'}^D F_{t-t'} + k_T^+ c \int_0^t dt' \psi_{t-t'}^P F_{t-t'} \left( 1 - e^{-r_{Pi}(t-t')} \right) \\ &\quad + k_T^+ c \int_0^t dt' \psi_{t-t'}^T F_{t-t'} \left( 1 - \frac{r_{Pi}}{r_{Pi} - r_H} e^{-r_H(t-t')} + \frac{r_H}{r_{Pi} - r_H} e^{-r_{Pi}(t-t')} \right) . \end{aligned} \quad (6)$$

Here the non-integral terms on the right hand sides represent change of tip status due to polymerization, depolymerization, hydrolysis, and phosphate release events at time  $t$ . The integral terms represent rates of reappearance of the monomer at the tip, weighted by factors accounting for the probability of hydrolysis or phosphate release during the time interval since the last appearance at the tip. For example, the first term on the right hand side of the first equation represents the rate of change of the probability of finding the ATP-actin monomer at the tip due to (i) polymerization of another monomer on top of it, (ii) depolymerization of the monomer itself, or (iii) hydrolysis of the ATP nucleotide bound to the monomer at the tip. The integral term on the right hand side represents reappearance events of the ATP-actin unit at the tip given that it got buried inside the filament due to a polymerization event at time  $t'$ , an event which occurred with rate  $k_T^+ c$ . Factor  $F$  represents the rate of reappearance of the buried monomer at the tip due to depolymerization of all the monomers which were added on top of it. The factor  $e^{-r_H(t-t')}$  is the probability that the ATP-actin monomer in question is not hydrolyzed while being buried.

Now the filament growth rate is given by

$$j = \begin{cases} v_D^- [1 - \int_0^\infty dt (\psi_t^D + \psi_t^P + \psi_t^T)] & (j < 0) \\ k_T^+ c - \int_0^\infty dt F_t & (j > 0) \end{cases} \quad (7)$$

Carrying out a Laplace transformation,  $t \rightarrow E$ ,  $F_t \rightarrow f_E$ , and  $\psi_t \rightarrow \Psi_E$  one has from eq. (7)

$$j = \begin{cases} v_D^- [1 - \Psi_0^D - \Psi_0^P - \Psi_0^T] & (j < 0) \\ k_T^+ c - f_0 & (j > 0) \end{cases} \quad (8)$$

while from eq. (6) one obtains

$$\begin{aligned} \Psi_E^T &= 1 / (E + v_T^- + r_H + k_T^+ c(1 - f_{E+r_H})) , \\ \Psi_E^P &= \frac{r_H + k_T^+ c r_H (f_{E+r_H} - f_{E+r_{Pi}}) / (r_{Pi} - r_H)}{E + v_P^- + r_{Pi} + k_T^+ c(1 - f_{E+r_{Pi}})} \Psi_E^T , \\ \Psi_E^D &= \frac{(r_{Pi} + k_T^+ c (f_E - f_{E+r_{Pi}})) \Psi_E^P + k_T^+ c (f_E - r_{Pi} f_{E+r_H}) / (r_{Pi} - r_H) + r_H f_{E+r_{Pi}} / (r_{Pi} - r_H)}{E + v_D^- + k_T^+ c(1 - f_E)} \Psi_E^T . \end{aligned} \quad (9)$$

Eliminating all  $\Psi$  in the Laplace transformation of eq. (5) after using eq. (9) one obtains the following recursive relationship involving the function  $f$  alone:

$$f_E = \mathcal{R}[f_{E+r_H}, f_{E+r_{Pi}}] , \quad (10)$$

where

$$\mathcal{R}[f_{E+r_H}, f_{E+r_{Pi}}] = \frac{-b_1 + \sqrt{b_1^2 - 4b_2 b_0}}{2b_2} . \quad (11)$$

Here the symbols  $b_0$ ,  $b_1$ , and  $b_2$  are functions of  $E$ ,  $f_{E+r_H}$  and  $f_{E+r_{P_i}}$  as follows:

$$\begin{aligned} b_0 &= A_{0,2}E^2 + A_{0,1}E + A_{0,0}, \\ b_1 &= A_{1,3}E^3 + A_{1,2}E^2 + A_{1,1}E + A_{1,0}, \\ b_2 &= A_{2,2}E^2 + A_{2,1}E + A_{2,0}, \end{aligned} \quad (12)$$

where

$$\begin{aligned} A_{0,2} &= -(r_H - r_{P_i})v_T^- k_T^+ c, \\ A_{0,1} &= (v_D^- r_H - r_{P_i}v_T^- + r_H(-v_P^- + v_T^-))(k_T^+ c)^2 f_{E+r_{P_i}} + (r_H v_P^- - v_D^- r_{P_i})(k_T^+ c)^2 f_{E+r_H} \\ &\quad - (r_H - r_{P_i})k_T^+ c(r_H v_P^- + v_T^-(v_D^- + v_P^- + r_{P_i} + 2k_T^+ c)), \\ A_{0,0} &= -v_D^-(r_H - r_{P_i})(k_T^+ c)^3 f_{E+r_{P_i}} f_{E+r_H} \\ &\quad - (r_H(v_P^- - v_T^-) + r_{P_i}v_T^-)k_T^+ c + v_D^-((r_H)^2 - r_{P_i}v_T^- + r_H(-r_{P_i} + v_T^- + k_T^+ c))(k_T^+ c)^2 f_{E+r_{P_i}} \\ &\quad + (r_H v_P^- k_T^+ c + v_D^-(r_H(v_P^- + r_{P_i}) - r_{P_i}(v_P^- + r_{P_i} + k_T^+ c)))(k_T^+ c)^2 f_{E+r_H} \\ &\quad - (r_H - r_{P_i})k_T^+ c(k_T^+ c(r_H v_P^- + v_T^-(v_P^- + r_{P_i} + k_T^+ c)) + v_D^-(r_H(v_P^- + r_{P_i}) + v_T^-(v_P^- + r_{P_i} + k_T^+ c))), \\ A_{1,3} &= r_H - r_{P_i}, \\ A_{1,2} &= -(r_H - r_{P_i})k_T^+ c(f_{E+r_{P_i}} + f_{E+r_H}) + (r_H - r_{P_i})(v_D^- + r_H + v_P^- + r_{P_i} + v_T^- + 3k_T^+ c), \\ A_{1,1} &= (r_H - r_{P_i})(k_T^+ c)^2 f_{E+r_{P_i}} f_{E+r_H} - (r_H - r_{P_i})(v_D^- + r_H + v_T^- + 2k_T^+ c)k_T^+ c f_{E+r_{P_i}} \\ &\quad - (r_H - r_{P_i})(v_D^- + v_P^- + r_{P_i} + 2k_T^+ c)k_T^+ c f_{E+r_H} \\ &\quad + (r_H - r_{P_i})(v_P^- v_T^- + r_{P_i}v_T^- + 2v_P^- k_T^+ c + 2r_{P_i}k_T^+ c + 3v_T^- k_T^+ c + 3(k_T^+ c)^2 \\ &\quad \quad + v_D^-(r_H + v_P^- + r_{P_i} + v_T^- + k_T^+ c) + r_H(v_P^- + r_{P_i} + 2k_T^+ c)), \\ A_{1,0} &= (r_H - r_{P_i})(v_D^- + k_T^+ c)(k_T^+ c)^2 f_{E+r_{P_i}} f_{E+r_H} \\ &\quad + (-v_D^-(r_H^2 - r_{P_i}v_T^- + r_H(-r_{P_i} + v_T^- + k_T^+ c)) \\ &\quad \quad + k_T^+ c(-r_H^2 + r_H(v_P^- + r_{P_i} - 2v_T^- - k_T^+ c) + r_{P_i}(2v_T^- + k_T^+ c)))k_T^+ c f_{E+r_{P_i}} \\ &\quad + (v_D^-(r_H(v_P^- + r_{P_i}) + r_{P_i}(v_P^- + r_{P_i} + k_T^+ c)) \\ &\quad \quad + k_T^+ c(r_{P_i}(v_P^- + r_{P_i} + k_T^+ c) - r_H(2v_P^- + r_{P_i} + k_T^+ c)))k_T^+ c f_{E+r_H} \\ &\quad + (r_H - r_{P_i})(v_D^-(r_H(v_P^- + r_{P_i}) + v_T^-(v_P^- + r_{P_i} + k_T^+ c)) \\ &\quad \quad + k_T^+ c(r_H(2v_P^- + r_{P_i} + k_T^+ c) + (v_P^- + r_{P_i} + k_T^+ c)(2v_T^- + k_T^+ c))), \\ A_{2,2} &= r_{P_i} - r_H, \\ A_{2,1} &= (r_H - r_{P_i})k_T^+ c(f_{E+r_{P_i}} + f_{E+r_H}) - (r_H - r_{P_i})(r_H + v_P^- + r_{P_i} + v_T^- + 2k_T^+ c), \\ A_{2,0} &= -(r_H - r_{P_i})(k_T^+ c)^2 f_{E+r_{P_i}} f_{E+r_H} + (r_H - r_{P_i})(r_H + v_T^- + k_T^+ c)k_T^+ c f_{E+r_{P_i}} \\ &\quad + (r_H - r_{P_i})(v_P^- + r_{P_i} + k_T^+ c)k_T^+ c f_{E+r_H} - (r_H - r_{P_i})(v_P^- + r_{P_i} + k_T^+ c)(r_H + v_T^- + k_T^+ c). \end{aligned} \quad (13)$$

We remark that eq. (11) is the solution of a quadratic equation; which of the two solutions of the quadratic is meaningful is easily checked by demanding  $f < 1$  in the  $E \rightarrow \infty$  limit.

Now for any given monomer concentration  $c$ , with the boundary condition  $f_E \rightarrow 0$  as  $E \rightarrow \infty$ , we started from a large enough  $E$  value and evolved eq. (10) towards  $E = 0$  to obtain  $f_0$ ,  $f_{r_{P_i}}$ , and  $f_{r_H}$ . Substituting these values in eq. (9) we further obtained  $\Psi_0^T$ ,  $\Psi_0^P$  and  $\Psi_0^D$ . Thus, given  $f_0$ ,  $\Psi_0^T$ ,  $\Psi_0^P$  and  $\Psi_0^D$  we evaluated  $j(c)$  using eq. (8). It was shown that this method converges to a unique solution provided one starts the evolution from large enough  $E$ , retaining a sufficient number of significant digits.

## B. Preaveraging Approximation: Calculation of Growth Rates.

In this part of the supporting material we present the method we used to calculate cap sizes and growth rates based on a preaveraging approximation. As discussed in the main text, compared to the exact calculations, this method gives different results for the cap size below  $c_{\text{crit}}$ , but provides very good approximations to growth rates. We denote  $\phi_T(n)$ ,  $\phi_P(n)$  and  $\phi_D(n)$  the probability that the  $n^{\text{th}}$  monomer away from the tip binds ATP, ADP-Pi or ADP, respectively. Consider first the tip, i. e.  $n = 1$ . One has [31]

$$\frac{d}{dt}\phi_T(1) = k_T^+ c[\phi_P(1) + \phi_D(1)] + [v_P^- \phi_P(1) + v_D^- \phi_D(1)]\phi_T(2) - v_T^- [\phi_P(2) + \phi_D(2)]\phi_T(1) - r_H \phi_T(1). \quad (14)$$

The first term on the right hand side represents change of tip status into ATP-actin due to polymerization of ATP-actin at an ADP-Pi-actin or ADP-actin tip. The second term represents change of tip status into ATP-actin due to (i) depolymerization of ADP-Pi-actin or ADP-actin at  $n = 1$ , and (ii) exposure of ATP-actin, previously buried at position  $n = 2$ . Within the preaveraging



approximation, the joint probability of ADP at  $n = 1$  and simultaneously ATP at  $n = 2$ , for example, is approximated as a product of probabilities:  $\phi_{DT}(1, 2) \approx \phi_D(1) \phi_T(2)$  in eq. (14). Similarly, the third term on the right hand side represents depolymerization of ATP-actin while the last term is change due to hydrolysis.

For ADP-Pi-actin one has similarly

$$\frac{d}{dt} \phi_P(1) = [v_T^- \phi_T(1) + v_D^- \phi_D(1)] \phi_P(2) - \{v_P^- [\phi_T(2) + \phi_D(2)] + k_T^+ c + r_{Pi}\} \phi_P(1) + r_H \phi_T(1) . \quad (15)$$

The analogous equations for  $n > 1$  are [31]

$$\begin{aligned} \frac{d}{dt} \phi_T(n) &= k_T^+ c [\phi_T(n-1) - \phi_T(n)] + [v_T^- \phi_T(1) + v_D^- \phi_D(1) + v_P^- \phi_P(1)] [\phi_T(n+1) - \phi_T(n)] - r_H \phi_T(n) \\ \frac{d}{dt} \phi_P(n) &= k_T^+ c [\phi_P(n-1) - \phi_P(n)] + [v_T^- \phi_T(1) + v_D^- \phi_D(1) + v_P^- \phi_P(1)] [\phi_P(n+1) - \phi_P(n)] \\ &+ r_H \phi_T(n) - r_{Pi} \phi_P(n) \quad (n > 1) \end{aligned} \quad (16)$$

The rate of change of the ADP-actin probabilities are determined from  $\phi_T(n) + \phi_P(n) + \phi_D(n) = 1$ . Starting from an arbitrary nucleotide profile and using long filaments, we evolved numerically eqs. (14)-(16) for a long enough time to allow the profile to reach its steady state (note that an analytical solution is also possible since (16) is linear, except for the tip terms [31]). The growth rate and the cap size were calculated from

$$N_{\text{cap}} = \sum_{n=1}^{\infty} \phi_T(n) + \phi_P(n), \quad N_{\text{cap}}^{\text{ATP}} = \sum_{n=1}^{\infty} \phi_T(n), \quad j = k_T^+ c - v_T^- \phi_T(1) - v_P^- \phi_P(1) - v_D^- \phi_D(1) . \quad (17)$$

### C. Analytical Calculation of Length Diffusivity as a Function of Concentration.

Here we prove that  $D_{\infty}(c)$  in fig. 6 has a sawtooth shape in the special case  $v_P^- = v_T^-$  and  $r_{Pi} \rightarrow 0$ . Consider first shrinking barbed ends,  $c < c_{\text{crit}}$ . For long times,  $t \gg t_{\text{cap}}$ , apart from fluctuations in the size of the steady state ATP/ADP-Pi cap, fluctuations in tip displacement are due to fluctuations in how far the ADP core has shrunk. Let us call  $u(\tau|t)$  the probability that in time  $t$  the filament is uncapped for a total time  $\tau$ . The probability that  $N$  monomers have been lost during this time is

$$p(N, t) = \int_0^{\infty} d\tau u(\tau|t) \mathcal{P}(N, v_D^- \tau), \quad \mathcal{P}(N, x) \equiv x^N e^{-x} / N!, \quad (18)$$

where the Poisson distribution,  $\mathcal{P}$ , describes the probability distribution of the number of depolymerized ADP-actin monomers during the total uncapped period. Let us evaluate  $u$  by noting that the average value of  $\tau$  and its second moment are given by

$$\langle \tau \rangle = t S_{\infty}, \quad \langle \tau^2 \rangle = 2S_{\infty} \int_0^t dt' \int_{t'}^t S(t'' - t') dt'', \quad (19)$$

for long enough times. Here  $S(t)$  is a return probability, namely the probability that the tip is uncapped at time  $t$ , given that it was uncapped at  $t = 0$ , and  $S(t) \rightarrow S_{\infty}$  for  $t \rightarrow \infty$ . To prove eq. (19), define  $\xi(t''|t')$  to be a random variable which is zero (unity) when the tip is capped (uncapped) at time  $t''$ , given it was uncapped at  $t'$ . One has  $\langle \tau^2 \rangle = \int_0^t \int_0^t dt' dt'' \langle \xi(t'|0) \xi(t''|0) \rangle = 2 \int_0^t dt' \int_{t'}^t dt'' \langle \xi(t'|0) \rangle \langle \xi(t''|t') \rangle$ . Noting that  $S(t) = \langle \xi(t|0) \rangle$  one recovers eq. (19).

Now the exact result for  $S$  is [30]

$$S(t) = e^{-(k_T^+ c + v_T^-) t} [I_0(2tx) + y^{-1/2} I_1(2tx) + (1 - y) \sum_{j=2}^{\infty} y^{-j/2} I_j(2tx)], \quad y \equiv k_T^+ c / v_T^-, \quad x \equiv (k_T^+ c v_T^-)^{1/2}, \quad (20)$$

where  $I_j$  are modified Bessel functions. Using  $S_{\infty} = 1 - c/c_{\text{crit}}$  one obtains for long times  $\langle \tau \rangle = t(1 - c/c_{\text{crit}})$  and  $\langle \tau^2 \rangle_c = (t/v_T^-)$  where  $\langle \rangle_c$  denotes second cumulant. Thus relative fluctuations in  $\tau$  become small for long times and  $u$  becomes Gaussian,  $u(\tau|t) \approx \text{const.} \exp[-(\tau - \langle \tau \rangle)^2 / (2 \langle \tau^2 \rangle_c)]$ . Substituting  $u$  in  $p(N, t)$  of eq. (18) and performing the integration one obtains

$$D_{\infty}(c) = \begin{cases} (v_D^-/2)[1 + (2v_D^-/v_T^- - 1)c/c_{\text{crit}}] & (c < c_{\text{crit}}) \\ (k_T^+ c + v_T^-)/2 & (c > c_{\text{crit}}) \end{cases} \quad (21)$$

which is the sawtooth curve plotted in fig. 6. Notice that  $D_{\infty}$  decreases for smaller concentrations since at  $c = 0$  one must recover the Poissonian fluctuations of a pure depolymerization process for which  $D_{\infty} = v_D^-/2$ . In eq. (21), the  $c > c_{\text{crit}}$  expression represents the fluctuations of a polymerization process of identical subunits [34] (since in the limit considered here the cap is never lost above  $c_{\text{crit}}$ ).